Geophysical Research Letters

RESEARCH LETTER
10.1029/2019GL082132

Separation of Methane Emissions From Agricultural and Natural Gas Sources in the Colorado Front Range

Natalie Kille[1,2], Randall Chiu[2,3], Matthias Frey[4], Frank Hase[4], Mahesh K. Sha[4,5], Thomas Blumenstock[4], James W. Hannigan[6], Johannes Orphal[4], Daniel Bon[7], and Rainer Volkamer[1,2,3]

[1]Department of Atmospheric and Oceanic Sciences, University of Colorado Boulder, Boulder, CO, USA, [2]CIRES, University of Colorado Boulder, Boulder, CO, USA, [3]Department of Chemistry, University of Colorado Boulder, Boulder, CO, USA, [4]Institute of Meteorology and Climate Research, Karlsruhe Institute of Technology, Karlsruhe, Germany, [5]Now at Royal Belgian Institute for Space Aeronomy, Brussels, Belgium, [6]Atmospheric Chemistry Observations and Modeling Laboratory, National Center for Atmospheric Research, Boulder, CO, USA, [7]Colorado Department of Public Health and Environment, Boulder, CO, USA

Abstract This proof-of-concept study demonstrates that methane (CH_4) emissions from natural gas (NG) and agriculture can be disentangled using the concept of excess column observations. A network of cost-effective sensors measured excess column-averaged dry-air mole fractions for CH_4 (ΔXCH_4), ethane (ΔXC_2H_6 as NG tracer), and ammonia (ΔXNH_3 from agriculture) in the Denver-Julesburg Basin during March 2015. ΔXCH_4 varied up to 17 ppb and was >3 times higher with winds from directions where NG is produced. The ΔXCH_4 variance is explained by variations in the C_2H_6-NH_3 tracer pair, attributing 63 ± 17% to NG, 25 ± 10% to agriculture, and 12 ± 12% to other sources. The ratios $\Delta XC_2H_6/\Delta XCH_4$ (16 ± 2%; indicates wet NG) and $\Delta XNH_3/\Delta XCH_4$ (43 ± 12%) were compatible with in situ measured ratios. Excess columns are independent of boundary layer height, characterize gases in the open atmosphere, are inherently calibrated, average over extended spatial scales, and provide a complementary perspective to quantify and attribute CH_4 emissions on regional scales.

Plain Language Summary Methane is the second most important anthropogenic greenhouse gas. Knowledge about methane sources is increasingly relevant as energy production continues to shift toward natural gas and becomes complicated by collocated emissions from natural gas production and agriculture due to shared land use. There is a need for methods to better decouple emissions from multiple sources that contribute to local enhancements in methane, which are small compared to the regional methane background concentrations, and depend on atmospheric transport and planetary boundary layer height. In this study, we show that the concept of collocated excess column measurements of methane and chemical tracers shows great promise as a viable approach to disentangle methane emissions from multiple sources by means of cost-effective networks of ground-based sensors. Excess columns are independent of boundary layer height, which makes quantification and source attribution of methane more straightforward.

Key Points:
- Methane emissions from natural gas and agriculture can be separated using the concept of excess column measurements of source tracers
- Column integrals over boundary layer height are complementary to in situ methods and useful to quantify and source apportion methane on regional scales
- Natural gas sources dominate over agricultural and other sources, but the latter are relatively more important when excess CH_4 is smaller than 5 ppb

Supporting Information:
- Supporting Information S1

Correspondence to:
R. Volkamer,
rainer.volkamer@colorado.edu

Citation:
Kille, N., Chiu, R., Frey, M., Hase, F., Sha, M. K., Blumenstock, T., et al. (2019). Separation of methane emissions from agricultural and natural gas sources in the Colorado Front Range. *Geophysical Research Letters*, *46*, 3990–3998. https://doi.org/10.1029/2019GL082132

Received 30 OCT 2018
Accepted 10 MAR 2019
Accepted article online 21 MAR 2019
Published online 4 APR 2019

1. Introduction

Methane (CH_4) is a major greenhouse gas in the atmosphere (Intergovernmental Panel on Climate Change, 2014). Globally, CH_4 sources can generally be grouped as biogenic, thermogenic, and pyrogenic; biogenic sources include wetlands, ruminants, and waste such as landfills; thermogenic sources are from fossil fuel combustion and the surface via coal and oil and natural gas (NG) extraction; or pyrogenic sources include wildfires and combustion of biomass (Kirschke et al., 2013; Saunois et al., 2016).

In Colorado, the dominating CH_4 sources are the NG industries, coal mining, and agriculture (which includes concentrated animal feeding operations [CAFOs]), with coal mining only occurring in the western part and not in the Front Range area (Arnold et al., 2014; Petron et al., 2012). Other sources in the state include waste combustion, landfills, and wastewater treatment facilities. According to Arnold et al. (2014), NG accounts for 38.5% of CH_4 emissions statewide, coal mining for 28.9%, agriculture for 22.3%, waste and landfills combined for 8.4%, and remaining sources for <2%.

Past studies in the Denver-Julesburg Basin (DJB) aiming to apportion CH_4 by agricultural and NG sources are based on in situ measurements and inventories and used carbon isotope ratios such as ^{13}C:^{12}C and

hydrocarbons such as C_2H_6 (Smith et al., 2015). Here we present the first source apportionment of CH_4 from agricultural sources and NG using the concept of excess columns. Excess columns are vertical columns from which a regional vertical column background has been subtracted. Other studies have used the concept of excess columns to quantify CH_4 emissions (Viatte et al., 2017; Wennberg et al., 2012), but this requires coupling with a chemical transport model, which is beyond the scope of this study. Column measurements can also be used to determine emission estimates through a combination of enhancement ratios and emission inventories (Wunch et al., 2009) or long-term trends of enhancement ratios (Franco et al., 2016; Hausmann et al., 2016). However, we are not aware of a previous attempt to source apportion CH_4 emissions using collocated measurements of source tracers. Unique tracers from the NG industry and agriculture/CAFOs are ethane (C_2H_6) and ammonia (NH_3), respectively. Even though the agricultural processes responsible for CH_4 emissions are distinct from those emitting NH_3, the sources are collocated within CAFOs, and CH_4 and NH_3 enhancements have been shown to correlate downwind, on a regional scale (van Haarlem et al., 2008). Measurements of C_2H_6 and NH_3 are used in this study to separate the CH_4 emissions from those two sources.

Figure 1a shows the locations of oil wells in the DJB and CAFOs in Northern Colorado, indicating that the CH_4 emissions from agricultural sources and NG are co-located. Boulder, Westminster, and Eaton in Colorado indicated as stars represent the measurement sites. With winds predominantly from the south during daytime in spring, the Eaton site is located inside the Front Range CH_4 hotspot, and the Boulder and Westminster sites are considered background sites. We perform a linear regression analysis similar to Garcia et al. (2006) to separate the excess CH_4 columns in terms of excess NH_3 and C_2H_6 columns to determine the source. Using the excess C_2H_6 columns, and for agricultural sources corrected excess CH_4 columns, we are able to determine the NG source type.

2. Method

2.1. Measurement Setup

A mininetwork of four instruments was located at three different sites: one central measurement site in Eaton, CO, inside the DJB, and two background measurement sites outside the DJB in Boulder and Westminster, CO. The deployment period was from 14 to 23 March 2015, of which five clear days provided simultaneous measurements from all four instruments: 14, 15, 16, 22, and 23 March. Three COCCON (Collaborative Carbon Column Observing Network; Frey et al., 2019) type EM27/SUN from the Karlsruhe Institute of Technology, Germany, measured CH_4 and oxygen (O_2) at each of the three sites. In addition, the University of Colorado mobile Solar Occultation Flux (CU mobile SOF) instrument measured C_2H_6 and NH_3 in Eaton, CO. All instruments use direct sunlight to measure the trace gas absorption along the direct solar beam and infer the vertical column density (VCD) of an absorber gas above the site. Eaton is located 11 km north of Greeley, CO (Weld County). The temperature ranged from 8 to 28 °C (median and mean: 21 °C) at the Greeley-Weld County Airport and surface wind speed ranged from 1.5 to 13.9 m/s (median: 4.1, mean: 5.6 m/s), coming mostly from the South (median direction of 175°).

The background measurement sites Boulder and Westminster are located distant from the area in which most CAFO sites and NG wells are located. Surface winds ranged from 1.5 to 9.3 m/s (median: 2.6, mean: 3.1 m/s) in speed and had a median direction of 130° at the Boulder Municipal Airport and 2.1 to 7.7 m/s (median: 3.1, mean: 3.5 m/s) in speed and 150° in median direction at the Rocky Mountain Metropolitan Airport in Broomfield, CO, making these sites suitable to determine background measurements.

2.2. Retrievals

The EM27/SUN spectrometer is described in more detail in Gisi et al. (2012), Frey et al. (2015), and Hase et al. (2016). CH_4 is retrieved from EM27/SUN solar spectra (5,000–11,000 cm^{-1}) using the spectral region at 5,897–6,145 cm^{-1} and O_2 at 7,765–8,005 cm^{-1} (Frey et al., 2015); the PROFFIT code is used for the retrievals (Hase et al., 2004). The ratio of CH_4 over O_2 cancels systematic errors; therefore, the precision for XCH_4 (see equations (1)–(2) below for definition) is higher than for the VCD. The single sounding precision of XCH_4 for 10 coadded scans is ~0.33 ppbv based on Hedelius et al. (2016; did not coadd scans).

The CU SOF instrument uses a custom-built digital solar tracker (Baidar et al., 2016), and is described in detail in Kille et al. (2017), where a detailed characterization of the NH_3 and C_2H_6 retrievals is also

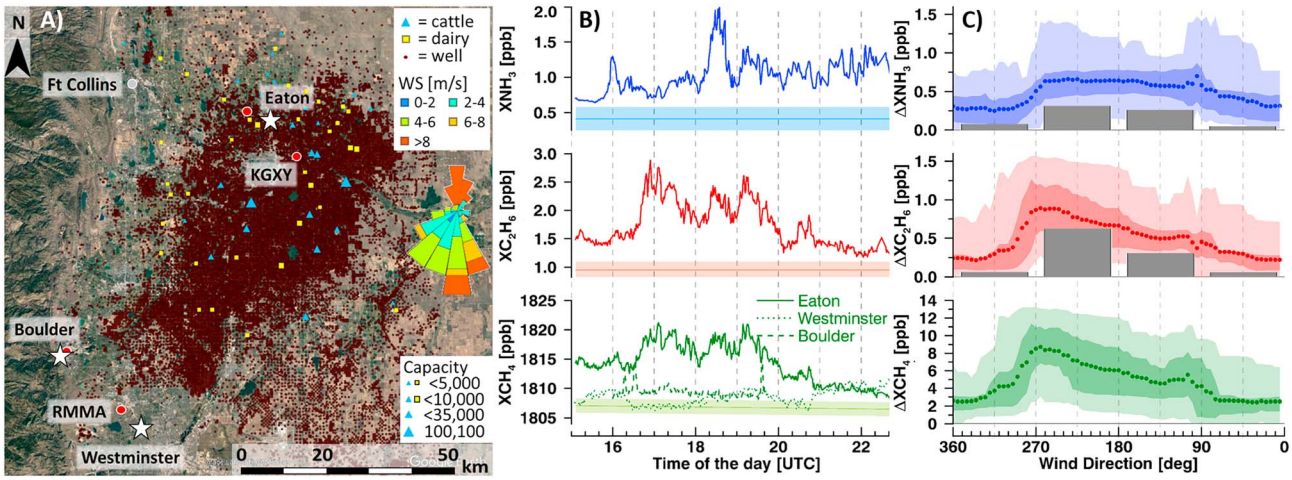

Figure 1. (a) Measurement setup in context of cattle and dairy feedlots, natural gas permits, and fracking wells in the Colorado Front Range. The wind rose indicates observed winds near the Eaton site during the entire measurement period. The Greeley-Weld County Airport (KGXY), a wind measurement location near Eaton, the Rocky Mountain Metropolitan Airport (RMMA), and the Boulder Municipal Airport are indicated by red circles (background image from Google Earth 2018). (b) Dry-air mole fractions of NH_3 (blue), C_2H_6 (red), CH_4 (green), and their background values (solid lines) and uncertainties (shading) on 14 March 2015 (see text for details on instruments deployed at measurement and background sites). (c) Campaign ΔXNH_3 (blue), ΔXC_2H_6 (red), and ΔXCH_4 (green) as a function of wind direction (wind from north = 0°, wind from east = 90°, etc.). Light shading corresponds to 5th and 95th percentiles, darker shading to 25th and 75th percentiles; the dots represent the mean value. The gray bars in the ΔXNH_3 panel represent CAFO emissions, and the gray bars in the ΔXC_2H_6 panel represent natural gas emissions (see text for details).

presented. Briefly, NH_3 is retrieved from CU SOF solar spectra (700–5,000 cm^{-1}) using the spectral region at 950–980 cm^{-1} and C_2H_6 at 2,970–3,000 cm^{-1}; the SFIT4 retrieval code is used for the retrievals (Hase et al., 2004). The precision of XNH_3 is 0.03 ppbv, and the precision of XC_2H_6 is 0.03 ppbv (using a campaign mean and median O_2 VCD of 3.90×10^{24} molec/cm^2).

Dry-air mole fractions (XGas) are derived from VCDs as

$$\mathrm{XGas} = 0.2095 \cdot \frac{\mathrm{VCD(Gas)}}{\mathrm{VCD(O_2)}}. \quad (1)$$

Furthermore, XCH_4 is divided by a calibration factor and scaled by a correction factor correcting for an air mass-dependent artifact that has been shown in Wunch et al. (2010) and Frey et al. (2015), see equation (2). This correction is dependent on solar zenith angle (SZA) θ and is <0.1% for XCH_4, insignificant for XO_2, and deemed irrelevant for XNH_3 and XC_2H_6

$$\mathrm{XCH_{4,corr}}(\theta) = \frac{\mathrm{XCH_4}(\theta)}{0.9765} \cdot \left\{ 1 + 3.796 \cdot 10^{-3} \cdot \left[\left(\frac{\theta + 16.04}{90 + 16.04} \right)^2 - \left(\frac{45 + 16.04}{90 + 16.04} \right)^2 \right] \right\}. \quad (2)$$

The enhancement over background concentrations is determined by

$$\Delta\mathrm{XGas} = \mathrm{XGas} - \mathrm{XGas_{BKG}}, \quad (3)$$

where $XCH_{4,BKG}$ is determined on a daily basis as the second percentile of pooled time series data from the three measurement locations and $XNH_{3,BKG}$ and $XC_2H_{6,BKG}$ are determined as a constant, equal to the second percentile of data from all measurements in Eaton, CO. The values derived for $XCH_{4,BKG}$ are insensitive to the choice of the first, second, and fifth percentiles (0.000 to 0.004 ppb change for $XCH_{4,BKG}$); $XNH_{3,BKG}$ changed by 0.010 ppb (second to fifth percentiles) and 0.040 ppb (first to second percentiles), and $XC_2H_{6,BKG}$ changed by 0.030 ppb (first to second as well as second to fifth percentiles). The choice to use the second percentile was based on the desire to maximize statistics and to determine slightly lower background values, but use of other percentiles would yield the same overall results. XCH_4 at background sites is 1.5 to 3% lower than the 1858 ppb CH_4 at the Mouna Loa Observatory (MLO) in Hawaii during March

2015. This low bias is partially due to (lower) stratospheric CH_4 and includes ~1% spectroscopic bias (Wunch et al., 2010). This uncertainty cancels out in calculating ΔXCH_4 and does not affect the further analysis. The XNH_3 and XC_2H_6 backgrounds determined by this method correspond to $(0.76 \pm 0.32) \times 10^{16}$ molec/cm^2 NH_3 and $(1.77 \pm 0.28) \times 10^{16}$ molec/cm^2 C_2H_6 and are within error identical with the regional minimum values of 0.5×10^{16} molec/cm^2 NH_3 and 1.5×10^{16} molec/cm^2 C_2H_6 in Kille et al. (2017).

2.3. Data Analysis

The statistical data analysis software Stata (v14.1) was used to perform a linear regression analysis on the time series of ΔXGas using the following equation:

$$\Delta XCH_4 = \beta_0 + \beta_1 \cdot \Delta XC_2H_6 + \beta_2 \cdot \Delta XNH_3. \quad (4)$$

Regression parameters β_1 and β_2 have units of [ppb/ppb] and represent the $\Delta CH_4/\Delta C_2H_6$ and $\Delta CH_4/\Delta NH_3$ ratios at the source, respectively; β_0 is excess XCH_4 in units of [ppb] that exceeds the regional background XCH_4 and could not be attributed to one of the two sources.

Sensitivity studies that varied in the constraints to β_i ($i = 0,1,2$) were performed: (I) no constraints, (II) only positive β_i, (III) β_1 and β_2 positive (β_0 unconstrained), (IV) only β_2 positive (β_0, β_1 unconstrained), and (V) β_0 held constant (β_1, β_2 unconstrained). For quality assurance nonphysical results, that is, $\beta_i < 0$, or $R^2 < 0.5$, were filtered out. Test (I) indicated that $\beta_0 = 0.64$ ppb and in test (V) the same value obtained the best R^2 (see Table S1 and Figure S1). The overall uncertainty on β_0 was determined as three times the standard deviation of β_0 from tests (I)–(IV). The uncertainties on β_1 and β_2 are the 95% confidence intervals from the linear regression analysis. In the final analysis β_0 is held constant and the quality-assured regression parameters taken from test (V) to allow for a better statistic compared to using test (I) (see Table S1) and resulted in $\beta_0 = 0.64 \pm 0.64$ ppb, $\beta_1 = 6.20 \pm 0.81$ ppb/ppb, and $\beta_2 = 2.34 \pm 0.65$ ppb/ppb (dashed lines in Figures 2 and S2). Figure S1 indicates that the choice of β_0 does not significantly change the percent-contribution from NG, agriculture, and other sources on CH_4 emissions. Possible error sources and an explanation for β_0 are discussed in section 3.2.

The β_i parameters were used to calculate percent-contributions of NG, agricultural, and other sources as follows:

$$\%\mathrm{NG} = \frac{\beta_1 \cdot \Delta XC_2H_6}{\beta_0 + \beta_1 \cdot \Delta XC_2H_6 + \beta_2 \cdot \Delta XNH_3}, \quad (5)$$

$$\%\mathrm{Agr} = \frac{\beta_2 \cdot \Delta XNH_3}{\beta_0 + \beta_1 \cdot \Delta XC_2H_6 + \beta_2 \cdot \Delta XNH_3}, \quad (6)$$

$$\%\mathrm{Other} = \frac{\beta_0}{\beta_0 + \beta_1 \cdot \Delta XC_2H_6 + \beta_2 \cdot \Delta XNH_3}. \quad (7)$$

NG and CAFO emission information is represented as gray bars relative to the measurement site in Figure 1c. It is calculated as an effective distance that expresses in which geographic direction the source of interest is located weighted by the probability of wind coming from that direction during the data analysis period. Information about the feedlot locations and maximum head counts for Colorado in 2014 were provided by D. Bon at the Colorado Department of Public Health and Environment (CDPHE), and NG facility emissions were extracted from Environmental Protection Agency's FLIGHT tool (http://ghgdata.epa.gov/ghgp). The effective distance is based on the inverse distance weight (IDW):

$$\mathrm{IDW}(\alpha) = \frac{\sum_i \frac{Z_i(\alpha)}{x_i}}{\sum_i \frac{1}{x_i}}, \quad (8)$$

where Z_i is the strength of source i and x_i is the distance between source i and the measurement site. A proxy for expected emissions transported to the measurement site from a subset of azimuth directions is obtained as

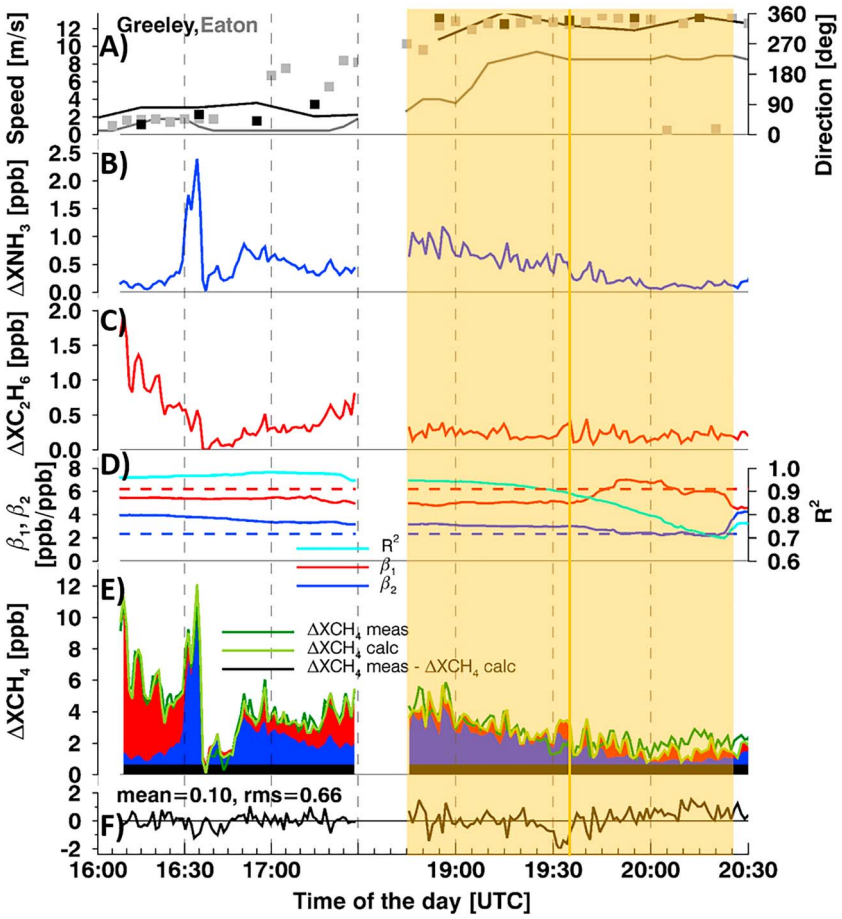

Figure 2. Time series data for 16 March 2015. (a) Wind speed and direction, (b and c) ΔXNH_3 and ΔXC_2H_6, the inputs of the statistical analysis; (d) linear regression parameters β_1, β_2, and R^2 from the statistical analysis; (e) measured and calculated ΔXCH_4 with shading below the calculated ΔXCH_4 that indicates contributions due to ΔXC_2H_6 and ΔXNH_3 (see text for details); (f) residual, the difference between measured and calculated ΔXCH_4. The yellow highlighted period demonstrates the rolling time period in form of number of points over which the instantaneous regression was performed.

$$\text{Proxy}\quad \text{Emission}(\alpha_i + \Delta\alpha) = \text{IDW}(\alpha_i + \Delta\alpha)\cdot f(\alpha_i + \Delta\alpha), \tag{9}$$

where (α_i+$\Delta\alpha$) denotes the subset of azimuth directions beginning at direction α_i and $IDW(\alpha_i+\Delta\alpha)$ and $f(\alpha_i+\Delta\alpha)$ are the IDW of sources and frequency of wind directions located within the subset of azimuth directions.

3. Results and Discussion

A map of the Colorado Front Range is shown in Figure 1a, which also shows the wind rose for the measurement times. Figure 1b shows an example of the column-averaged dry-air mole fractions (XGas; see equations (1) and (2)) from 14 March as well as background concentrations with their respective uncertainty. The excess columns ΔXGas calculated using equation (3) are shown as function of wind direction in Figure 1c. Also shown are the expected emissions of feedlots and NG facilities based on IWD calculations (see section 2.3). ΔXNH_3 is enhanced evenly from east (90°) to south (180°) to west (270°); ΔXC_2H_6 is enhanced increasingly from east to south to west. This wind direction dependence is consistent with that of the expected emissions to a first approximation. ΔXCH_4 generally resembles the wind direction

dependence of ΔXC_2H_6 more closely than that of ΔXNH_3—though both sources cannot be easily disentangled from a wind-direction-dependent analysis alone.

The approach for source apportionment is illustrated in Figure 2 for an example day (16 March 2015), when winds gradually shifted toward a northerly flow (wind direction of 180°). The regression parameters and calculated contributions of ΔXNH_3 and ΔXC_2H_6 to ΔXCH_4 are also shown; the full time series is included as Figure S2. Generally, when $R^2 > 0.8$ then β_1 was relatively constant. R^2 tends to decrease when ΔXCH_4 is low. The quality filter using $R^2 > 0.5$ was chosen to avoid eliminating too many data points.

Based on the regression parameters and observed tracer excess columns, ΔXCH_4 was calculated and compared to the observed ΔXCH_4. The mean and root-mean-square (rms) of the residual differences between observed and calculated ΔXCH_4 is shown in Figure 2 and in Figure S2 for each day. The overall mean = 0.10 ppb and rms = 0.87 during quality-assured periods, and during filtered out periods the mean = 0.07 ppb and rms = 1.34.

The filled polygons in Figure S2 indicate the contribution of ΔXC_2H_6 and ΔXNH_3 to the calculated ΔXCH_4. On 16 March ΔXCH_4 is smaller compared to 14 March, and the contribution of ΔXNH_3 is larger on 16 March compared to 14 March. The measured ΔXCH_4 median = 4.2 ppb, mean = 5.2 ppb, and max = 17.1 ppb. Figure S3 shows the change in percent-contribution as a function of ΔXCH_4; as ΔXCH_4 concentration increases so does the percent-contribution of NG emissions, whereas the percent-contribution from agricultural and other sources is more relevant during times of smaller ΔXCH_4. This matches the behavior in Figure 1c and establishes that both sources contribute to ΔXCH_4. It also emphasizes that during times of smaller observed ΔXCH_4 agricultural and other sources dominated the percent-contribution compared to times of higher ΔXCH_4 (>5 ppb) when NG dominated.

3.1. Comparison With the Literature

A few other studies that have apportioned (Peischl et al., 2018; Petron et al., 2014; Townsend-Small et al., 2016) or quantified (Eilerman et al., 2016; Fried et al., 2015; Gilman, 2017; Tzompa-Sosa et al., 2017; Yuan et al., 2017) CH_4 in the DJB study area exist, but none have attempted to source apportion CH_4 based on excess columns. These results can be used to assess how the concept of excess columns compares with results based on in situ observations. Based on the quality-assured linear regression parameters and the measurements of excess columns, 62.8 ± 17.1% of ΔXCH_4 is from NG sources, 25.4 ± 9.6% is from agricultural sources, and 11.8 ± 11.8% could not be attributed to a source. The attribution to NG agrees well with values reported in studies by Petron et al. (2014) for Weld County in May 2012 and Peischl et al. (2018) as shown in Table 1, where the dominating source of CH_4 is determined to be the NG sector. The data by Townsend-Small et al. (2016) remain somewhat ambiguous whether the majority of CH_4 is from NG or agriculture. The attribution to agriculture determined in this study falls between that from Petron et al. (2014) and Townsend-Small. However, it is to note that the Petron study took place a couple years earlier and the Townsend-Small study took place in a different season, indicating that the different outcomes are due to seasonal changes in the sources.

Two advantages of using remote sensing column measurements are that they are independent of boundary layer height and do not use inlets, which present a challenge regarding NH_3 partitioning to surfaces. Ground-based solar absorption measurements offer good vertical sensitivity across the whole atmosphere. This is further illustrated in Figure S4, where the column sensitivities for NH_3, C_2H_6, and CH_4 are compared with vertical profiles measured by in situ sensors during the Deriving Information on Surface Conditions from Column and Vertically Resolved Observations Relevant to Air Quality (DISCOVER-AQ; July/August 2014) and Shale Oil and Natural Gas Nexus (SONGNEX; March/April 2015) field campaigns. The median column sensitivity below 4.8 (2.4) km is 1.07 ± 0.04 (1.03 ± 0.04) for NH_3, 1.04 ± 0.03 (1.01 ± 0.03) for C_2H_6, and 1.05 ± 0.03 (1.06 ± 0.03) for CH_4 (errors indicate SZA variability for data used in this study; 42° < SZA < 70°). Most of the excess column resides in the lowest kilometer, and >99% resides below 4.8 km above sea level (or 550 mbar) for all gases. At higher altitudes, CH_4 during SONGNEX (same month as our study) agrees closely with the median CH_4 measured at MLO. Changes in free tropospheric mixing ratios contribute relatively less to the excess columns, since they are weighted by lower density. Figure S4 demonstrates that the vertical distributions are similar for the three gases and that the column sensitivities

Table 1
Literature Comparison of CH_4 Source Attributions in the Colorado Front Range

Source attribution				
NG	Agriculture	Other	Study period	Reference
62.8 ± 17.1%	25.4 ± 9.6%	11.8 ± 11.8%	March 2015	This work
74%	15%	11%	May 2012	Petron et al. (2014)
31–61%	39–69%		July/August 2014	Townsend-Small et al. (2016)
75 ± 37%	—	—	March/April 2015	Peischl et al. (2018)

of individual instruments are virtually identical, and near unity for all gases at the altitudes that contribute to the excess columns.

We therefore believe that the consistency of excess columns as a complementary tool to in situ observations to source apportion CH_4 emissions on the regional scale can be evaluated by comparing the regression parameters β_1 and β_2 with the results from in situ observations in the literature. This is possible because the regression parameters β_1 and β_2 are directly indicative of the $\Delta XC_2H_6/\Delta XCH_4$ and $\Delta XNH_3/\Delta XCH_4$ ratios and have been determined as 16.1 ± 2.1% and 43 ± 12% in this study. Previous studies that have measured $\Delta C_2H_6/\Delta CH_4$ and $\Delta NH_3/\Delta CH_4$ using in situ sensors in the DJB are summarized and compared to our results in Table 2. There is excellent agreement with the aircraft study by Fried et al. (2015), and also Tzompa-Sosa et al. (2017). C_2H_6/CH_4 ratios reveal information about the source type; biogenic sources have a ratio of <0.2%, dry gas of 1 to 6%, wet gas >6%, pipeline grade NG <15%, and processed NG liquids >30% (Yacovitch et al., 2014). According to Smith et al. (2015) and Yacovitch et al. (2014) the $\Delta XC_2H_6/\Delta XCH_4$ = 16.1 ± 2.1% indicates that the NG source of CH_4 is wet gas. The NH_3/CH_4 ratio quantified based on excess columns in this work has robust error bars and tends to be compatible with the higher published values from previous in situ measurements. Altogether, the approach of quantifying and source apportioning CH_4 on the regional scale holds potential to decrease the error bars both of the ratios and the source attribution. A limiting factor in this work is the short study period.

3.2. Error Sources

Errors in the excess column method originate in the background correction and uncertainty on the regression parameters. The uncertainties on the background correction (included in Figure 1b) are 0.17 ppb on ΔXNH_3, 0.15 ppb on ΔXC_2H_6, and 0.62 ppb on ΔXCH_4, determined as the standard deviation between the data analysis days. The uncertainties on the background correction and the 95% confidence intervals on the regression parameters were propagated through equations (5)–(7) for the overall error of the source apportionment. In this study, the number of data analysis points was limited to 1,294, and the number of points determining the instantaneous β_i was set at 100. To decrease the 95% confidence intervals on the regression parameters using more than 100 points will increase the certainty of the source apportionment. A longer study with more measurement points would provide the data to determine how the wind direction affects the source apportionment.

The percent-contribution quantified due to the residual, β_0, of 11.8 ± 11.8% compared well with the attribution value in Petron et al. (2014) of 11% from landfills and wastewater plants. However, there is no unique

Table 2
Literature Comparison of Tracer Ratios to CH_4

$\Delta XC_2H_6/\Delta XCH_4$		$\Delta XNH_3/\Delta XCH_4$	
Ratio (%)	Reference	Ratio (%)	Reference
16.1 ± 2.1	This work	42.7 ± 11.9	This work
18.7 ± 3.2	Fried et al. (2015)	17 (9–30)	Eilerman et al. (2016)
17	Tzompa-Sosa et al. (2017)	~30–50	Yuan et al. (2017)
10.2 ± 0.2	Gilman (2017)	—	—

tracer from landfills and wastewater plants that could be measured and utilized in this study. Another possible explanation for the residual is tracer losses during transport; CH_4 and C_2H_6 have lifetimes on the order of 8–10 years (Hodnebrog et al., 2018; Lelieveld et al., 1998; Sherwen et al., 2016) and 2 months (Hodnebrog et al., 2018; Hough, 1991), whereas NH_3 has a much shorter atmospheric lifetime on the order of hours to a few days (Dentener & Crutzen, 1994; Gupta et al., 2003). Transport distances vary depending on the dry deposition velocity and height at which NH_3 is located in the vertical column. Assuming that NH_3 from feedlots further downwind of the measurement site has been deposited during transport, this would affect the regression parameters β_0 and β_1 and therefore overall source apportionment.

Altogether, the residual contribution $\beta_0 = 0.64$ ppb implies that the magnitude of this error impacting the result is small because the measured ΔXCH_4 varies up to 17.1 ppb.

Data

Data displayed in graphs are available from the following data archive: https://volkamergroup.colorado.edu/publications. DISCOVER-AQ data are available at: doi:10.5067/Aircraft/DISCOVER-AQ/Aerosol-TraceGas. SONGNEX data are available at: https://esrl.noaa.gov/csd/groups/csd7/measurements/2015songnex/P3/DataDownload/. MLO data are available at http://www.esrl.noaa.gov/gmd/obop/mlo/.

Acknowledgments
Financial support from National Science Foundation (NSF) grants AGS-1452317, AGS-1744537, and AGS-1754019 are gratefully acknowledged. Natalie Kille is recipient of a CIRES graduate fellowship. We acknowledge support by the ACROSS research infrastructure of the Helmholtz Association of German Research Centres (HGF). The Colorado Department of Public Health and Environment (CDPHE) helped fund the CU mobile SOF instrument during FRAPPE and provided the CAFO data. The authors thank Philip Handley for helping with the field deployment, NOAA ESRL and Dlugokencky et al. (2018) for CH_4 at MLO, two anonymous reviewers for helpful comments, and the DISCOVER-AQ and SONGNEX science teams for providing access to aircraft measurements of NH_3, C_2H_6, and CH_4. Specifically, we are grateful for Armin Wisthaler, Tara Yacovitch, Scott Herndon, Josh DiGangi, Sally Pusede, and Glenn Diskin for access to their DISCOVER-AQ data, and Scott Eilerman, Andy Neuman, Jeff Peischl, Tom Ryerson, and Joost de Gouw for the SONGNEX data.

References

Arnold, S., Dileo, J., & Takushi, T. (2014). Colorado greenhouse gas inventory—2014 update including projections to 2020 and 2030. Retrieved from https://www.colorado.gov/pacific/sites/default/files/AP-COGHGInventory2014Update.pdf

Baidar, S., Kille, N., Ortega, I., Sinreich, R., Thomson, D., Hannigan, J., & Volkamer, R. (2016). Development of a digital mobile solar tracker. *Atmospheric Measurement Techniques*, *9*(3), 963–972. https://doi.org/10.5194/amt-9-963-2016

Dentener, F. J., & Crutzen, P. J. (1994). A three-dimensional model of the global ammonia cycle. *Journal of Atmospheric Chemistry*, *19*(4), 331–369. https://doi.org/10.1007/BF00694492

Dlugokencky, E. J., Crotwell, A. M., Lang, P. M., Mund, J. W., & Rhodes, M. E. (2018). Atmospheric methane dry air mole fractions from quasi-continuous measurements at Barrow, Alaska and Mauna Loa, Hawaii, 1986–2017, Version: 2018-03-19. Retrieved from ftp://aftp.cmdl.noaa.gov/data/trace_gases/ch4/in-situ/surface/

Eilerman, S. J., Peischl, J., Neuman, J. A., Ryerson, T. B., Aikin, K. C., Holloway, M. W., et al. (2016). Characterization of ammonia, methane, and nitrous oxide emissions from concentrated animal feeding operations in northeastern Colorado. *Environmental Science & Technology*, *50*(20), 10,885–10,893. https://doi.org/10.1021/acs.est.6b02851

Franco, B., Mahieu, E., Emmons, L. K., Tzompa-Sosa, Z. A., Fischer, E. V., Sudo, K., et al. (2016). Evaluating ethane and methane emissions associated with the development of oil and natural gas extraction in North America. *Environmental Research Letters*, *11*(4), 044010. https://doi.org/10.1088/1748-9326/11/4/044010

Frey, M., Hase, F., Blumenstock, T., Groß, J., Kiel, M., Mengistu Tsidu, G., et al. (2015). Calibration and instrumental line shape characterization of a set of portable FTIR spectrometers for detecting greenhouse gas emissions. *Atmospheric Measurement Techniques*, *8*(7), 3047–3057. https://doi.org/10.5194/amt-8-3047-2015

Frey, M., Sha, M. K., Hase, F., Kiel, M., Blumenstock, T., Harig, R., et al. (2019). Building the COllaborative Carbon Column Observing Network (COCCON): long-term stability and ensemble performance of the EM27/SUN Fourier transform spectrometer. *Atmospheric Measurement Techniques*, *12*(3), 1513–1530. https://doi.org/10.5194/amt-12-1513-2019

Fried, A., Walega, J., Weibring, P., & Richter, D. (2015). Simultaneous formaldehyde and ethane measurements during the 2014 FRAPPE study. Paper presented at FRAPPE/DISCOVER-AQ Science Team Meeting, Boulder, CO.

Garcia, A. R., Volkamer, R., Molina, L. T., Molina, M. J., Samuelson, J., Mellqvist, J., et al. (2006). Separation of emitted and photochemical formaldehyde in Mexico City using a statistical analysis and a new pair of gas-phase tracers. *Atmospheric Chemistry and Physics*, *6*(12), 4545–4557. https://doi.org/10.5194/acp-6-4545-2006

Gilman, J. (2017). Airborne and ground-based measurements of emissions from oil and gas extraction and their impacts in the Colorado Front Range. Paper Presented at FRAPPE/DISCOVER-AQ Science Team Meeting, Boulder, CO.

Gisi, M., Hase, F., Dohe, S., Blumenstock, T., Simon, A., & Keens, A. (2012). XCO_2-measurements with a tabletop FTS using solar absorption spectroscopy. *Atmospheric Measurement Techniques*, *5*(11), 2969–2980. https://doi.org/10.5194/amt-5-2969-2012

Gupta, A., Kumar, R., Kumari, K. M., & Srivastava, S. S. (2003). Measurement of NO_2, NHO_3, NH_3 and SO_2 and related particulate matter at a rural site in Rampur, India. *Atmospheric Environment*, *37*(34), 4837–4846. https://doi.org/10.1016/j.atmosenv.2003.07.008

Hase, F., Frey, M., Kiel, M., Blumenstock, T., Harig, R., Keens, A., & Orphal, J. (2016). Addition of a channel for XCO observations to a portable FTIR spectrometer for greenhouse gas measurements. *Atmospheric Measurement Techniques*, *9*(5), 2303–2313. https://doi.org/10.5194/amt-9-2303-2016

Hase, F., Hannigan, J. W., Coffey, M. T., Goldman, A., Höpfner, M., Jones, N. B., et al. (2004). Intercomparison of retrieval codes used for the analysis of high-resolution, ground-based FTIR measurements. *Journal of Quantitative Spectroscopy and Radiative Transfer*, *87*(1), 25–52. https://doi.org/10.1016/j.jqsrt.2003.12.008

Hausmann, P., Sussman, R., & Smale, D. (2016). Contribution of oil and natural gas production to renewed increase in atmospheric methane (2007–2014): top-down estimate from ethane and methane column observations. *Atmospheric Chemistry and Physics*, *16*(5), 3227–3244. https://doi.org/10.5194/acp-16-3227-2016

Hedelius, J. K., Viatte, C., Wunch, D., Roehl, C. M., Toon, G. C., Chen, J., et al. (2016). Assessment of errors and biases in retrievals of X_{CO2}, X_{CH4}, X_{CO}, and X_{N2O} from a 0.5 cm^{-1} resolution solar-viewing spectrometer. *Atmospheric Measurement Techniques*, *9*(8), 3527–3546. https://doi.org/10.5194/amt-9-3527-2016

Hodnebrog, Ø., Dalsøren, S. B., & Myhre, G. (2018). Lifetimes, direct and indirect radiative forcing, and global warming potentials of ethane (C_2H_6), propane (C_3H_8), and butane (C_4H_{10}). *Atmospheric Science Letters*, *19*(2), 19. https://doi.org/10.1002/asl.804

Hough, A. M. (1991). Development of a two-dimensional global tropospheric model: Model chemistry. *Journal of Geophysical Research*, *96*(D4), 7325–7362. https://doi.org/10.1029/90JD01327

Intergovernmental Panel on Climate Change (2014). *Fifth Assessment Report*. Cambridge: Cambridge University Press.

Kille, N., Baidar, S., Handley, P., Ortega, I., Sinreich, R., Cooper, O. R., et al. (2017). The CU mobile solar occultation flux instrument: Structure functions and emission rates of NH_3, NO_2 and C_2H_6. *Atmospheric Measurement Techniques*, *10*(1), 373–392. https://doi.org/10.5194/amt-10-373-2017

Kirschke, S., Bousquet, P., Ciais, P., Saunois, M., Canadell, J. G., Dlugokencky, E. J., et al. (2013). Three decades of global methane sources and sinks. *Nature Geoscience*, *6*(10), 813–823. https://doi.org/10.1038/ngeo1955

Lelieveld, J., Crutzen, P. J., & Dentener, F. J. (1998). Changing concentration, lifetime and climate forcing of atmospheric methane. *Tellus*, *50*(2), 128–150. https://doi.org/10.1034/j.1600-0889.1998.t01-1-00002.x

Peischl, J., Eilerman, S. J., Neuman, J. A., Aikin, K. C., de Gouw, J., Gilman, J. B., et al. (2018). Quantifying methane and ethane emissions to the atmosphere from central and western U.S. oil and Natural gas production regions. *Journal of Geophysical Research: Atmospheres*, *123*, 7725–7740. https://doi.org/10.1029/2018JD028622

Petron, G., Frost, G., Miller, B. R., Hirsch, A. I., Montzka, S. A., Karion, A., et al. (2012). Hydrocarbon emissions characterization in the Colorado Front Range: A pilot study. *Journal of Geophysical Research*, *117*, D04304. https://doi.org/10.1029/2011JD016360

Petron, G., Karion, A., Sweeney, C., Miller, B. R., Montzka, S. A., Frost, G. J., et al. (2014). A new look at methane and nonmethane hydrocarbon emissions from oil and natural gas operations in the Colorado Denver-Julesburg Basin. *Journal of Geophysical Research: Atmospheres*, *119*, 6836–6852. https://doi.org/10.1002/2013JD021272

Saunois, M., Bousquet, P., Poulter, B., Peregon, A., Ciais, P., Canadell, J. G., et al. (2016). The global methane budget 2000–2012. *Earth System Science Data*, *8*(2), 697–751. https://doi.org/10.5194/essd-8-697-2016

Sherwen, T., Schmidt, J. A., Evans, M. J., Carpenter, L. J., Großmann, K., Eastham, S. D., et al. (2016). Global impacts of tropospheric halogens (Cl, Br, I) on oxidants and composition in GEOS-Chem. *Atmospheric Chemistry and Physics*, *16*(18), 12,239–12,271. https://doi.org/10.5194/acp-16-12239-2016

Smith, M. L., Kort, E. A., Karion, A., Sweeney, C., Hemdon, S. C., & Yacovitch, T. I. (2015). Airborne ethane observations in the Barnett Shale: Quantification of ethane flux and attribution of methane emissions. *Environmental Science & Technology*, *49*(13), 8158–8166. https://doi.org/10.1021/acs.est.5b00219

Townsend-Small, A., Botner, E. C., Jimenez, K. L., Schroeder, J. R., Blake, N. J., Meinardi, S., et al. (2016). Using stable isotopes of hydrogen to quantify biogenic and thermogenic atmospheric methane sources: A case study from the Colorado Front Range. *Geophysical Research Letters*, *43*, 11,462–11,471. https://doi.org/10.1002/2016GL071438

Tzompa-Sosa, Z. A., Mahieu, E., Franco, B., Keller, C. A., Turner, A. J., Helmig, D., et al. (2017). Revisiting global fossil fuel and biofuel emissions of ethane. *Journal of Geophysical Research: Atmospheres*, *122*, 2493–2512. https://doi.org/10.1002/2016JD025767

van Haarlem, R. P., Desjardins, R. L., Gao, Z., Flesch, T. K., & Li, X. (2008). Methane and ammonia emissions from a beef feedlot in western Canada for a twelve-day period in the fall. *Canadian Journal of Animal Science*, *88*(4), 641–649. https://doi.org/10.4141/CJAS08034

Viatte, C., Lauvaux, T., Hedelius, J. K., Parker, H., Chen, J., Jones, T., et al. (2017). Methane emissions from dairies in the Los Angeles Basin. *Atmospheric Chemistry and Physics*, *17*(12), 7509–7528. https://doi.org/10.5194/acp-17-7509-2017

Wennberg, P. O., Mui, W., Wunch, D., Kort, E. A., Blake, D. R., Atlas, E. L., et al. (2012). On the sources of methane to the Los Angeles atmosphere. *Environmental Science & Technology*, *46*(17), 9282–9289. https://doi.org/10.1021/es301138y

Wunch, D., Toon, G. C., Wennberg, P. O., Wofsy, S. C., Stephens, B. B., Fischer, M. L., et al. (2010). Calibration of the Total Carbon Column Observing Network using aircraft profile data. *Atmospheric Measurement Techniques*, *3*(5), 1351–1362. https://doi.org/10.5194/amt-3-1351-2010

Wunch, D., Wennberg, P. O., Toon, G. C., Keppel-Aleks, G., & Yavin, Y. G. (2009). Emissions of greenhouse gases from a North American megacity. *Geophysical Research Letters*, *36*, L15810. https://doi.org/10.1029/2009GL039825

Yacovitch, T. I., Herndon, S. C., Roscioli, J. R., Floerchinger, C., McGovern, R. M., Agnese, M., et al. (2014). Demonstration of an ethane spectrometer for methane source identification. *Environmental Science & Technology*, *48*(14), 8028–8034. https://doi.org/10.1021/es501475q

Yuan, B., Coggon, M. M., Koss, A. R., Warneke, C., Eilerman, S., Peischl, J., et al. (2017). Emissions of volatile organic compounds (VOCs) from concentrated animal feeding operations (CAFOs): chemical compositions and separation of sources. *Atmospheric Chemistry and Physics*, *17*(8), 4945–4956. https://doi.org/10.5194/acp-17-4945-2017